Cite as: J. Appl. Phys. 137, 214503 (2025); doi: 10.1063/5.0268604

Submitted: 3 March 2025 · Accepted: 10 May 2025 ·

Published Online: 3 June 2025







Weipeng Peng, 🛮 📵 Fei Liang, ¹Yangquan Liao, ¹Hongzhen Jing, ¹Ying Xiang, ¹,a) 📵 Péter Salamon, ²,a) 📵 Nándor Éber,² D Ágnes Buka,² D Ling Wang,³ Nemanja Trišović,⁴ D and Huaiping Zhang⁵ C

AFFILIATIONS

- ¹School of Information Engineering, Guangdong University of Technology, Guangzhou 510006, People's Republic of China
- ²HUN-REN Wigner Research Centre for Physics, P.O. Box 49, 1525 Budapest, Hungary
- School of Materials Science and Engineering, Tianjin University, 300350 Tianjin, People's Republic of China
- 4 Faculty of Technology and Metallurgy, University of Belgrade, Karnegijeva 4, 11120 Belgrade, Serbia
- ⁵Varitronix (He Yuan) Display Technology Co. Ltd, He Yuan 517000, People's Republic of China

ABSTRACT

Periodic flexoelectric domains (FDs) stimulated by both electric and optical fields were examined in a photosensitive chiral nematic liquid Periodic flexoelectric domains (FDs) stimulated by both electric and optical fields were examined in a process of FDs, by crystal. It was observed that the optical field is an excellent candidate to modulate the morphology and electric threshold voltage of FDs, by the included bulk effect through the optical control of chiraleither an optically induced surface effect through photo-alignment or an optically induced bulk effect through the optical control of chirality. With preset spatial patterns of the optical field, proof-of-concept prototypes of ring-shaped and fan-shaped gratings were constructed, which can be used in encoders to measure the angle directly and precisely.

© 2025 Author(s). All article content, except where otherwise noted, is licensed under a Creative Commons Attribution-NonCommercial 4.0 International (CC BY-NC) license (https://creativecommons.org/licenses/by-nc/4.0/). https://doi.org/10.1063/5.0268604

I. INTRODUCTION

Liquid crystals (LCs) are anisotropic materials possessing a preferred molecular orientation (the so-called director \mathbf{n}), which can be conveniently guided by an external electric, magnetic, or optical field, and surface alignment. As a result, LCs are widely utilized in electro-optic displays and photonic devices.

Meanwhile, LCs can self-assemble into spatially periodic structures in response to the stimuli of external fields.³⁻⁷ A typical example is the flexoelectric domain (FD), a static, spatially periodic director deformation under an electric field, which emerges due to the flexoelectric effect (FE).^{8,9} The FE manifests itself as an electric polarization, $\mathbf{P}_{\rm fl} = e_1 \mathbf{n} \, \text{div } \mathbf{n} - e_3 \mathbf{n} \times \text{curl } \mathbf{n}$, where e_1 and e_3 are phenomenological flexoelectric coefficients. When driven by an electric field, flexoelectric domains (FDs) emerge as a spatially periodic director distortion above a critical electric voltage U_{ϕ}^{-1} distortion-induced increase in the elastic and dielectric free energies is overcompensated by the free energy reduction (-Pf E) due to the flexoelectric interaction. Thus, for $U > U_c$, the periodically distorted state (the FDs) has a lower free energy than the initial undistorted one.

Usually, in nematic LCs, FDs appear as static longitudinal stripes with a periodicity of Λ , running parallel to the initial orientation n₀. It was reported that FDs exhibit a markedly voltagedependent $\Lambda_{3}^{15,16}$ upon increasing the voltage, Λ shrinks. This effect has recently been exploited to demonstrate beam steering functionality and has, thus, drawn special attention.¹⁷

While most of current efforts on FDs are focused on the tunability upon electric field, 19 the extension by including optical stimulus may bring about very surprising results; such an attempt has been performed on bent core nematic (BCN) molecules embedding an azo group; it made U_c become the function of the intensity and wavelength of the illuminating light.²⁴

Self-assembled FD stripes can be modulated by properly adjusting the external and internal conditions exerted by optical fields:

(1) Surface alignment, as an external condition, can be set via the optically induced surface effect using the photo-alignment technique. In fact, specific types of surface alignment, which yield the desired molecular orientation and director distribution, are

^{a)}Authors to whom correspondence should be addressed: frank_xiang68@qq.com and salamon.peter@wigner.hun-ren.hu

preconditions for all LC devices. The conventional methods for creating uniform homogeneous alignment involve the rubbing technique, where a velvet-type cloth comes into contact with a polymer-coated substrate. Although this contact rubbing technique is simple and effective in achieving LC alignment, it is permanent and irreversible, thus not flexible enough to implement inhomogeneous alignment with complex patterns. In contrast, photo-alignment, as an alternative alignment technique, is superior for the high-quality and high-resolution multi-domain orientation of LCs.²¹ Common photo-aligning layers used for this purpose are usually azobenzene-based compounds, which undergo trans-cis isomerization when irradiated with the polarized light of proper wavelength. 22,23 As the photosensitive layer is capable of aligning the nearby LC molecules, the resulting director distribution at the surface of LCs corresponds to the polarization pattern of the optical field.

(2) The helical structure of chiral nematics (CLCs), as an internal condition, can be altered by an optically induced bulk effect via the photo-tuning technique. Herein, a small amount of photosensitive chiral dopant is included to form a chiral nematic (cholesteric) with a pitch *P*. As the helical twisting power (*HTP*) of the chiral dopant changes in response to the light illumination, *P* of the CLC is a function of the light intensity *I*. ^{24–26} If *I* has a spatial distribution, the corresponding *P*(*I*) depends also on space.

In this paper, we propose a well-designed photosensitive LC system, which is composed of a photosensitive CLC filled into a hybrid-aligned (HA) cell with a photosensitive substrate. By virtue of a flexible and dynamic optical setup, commanding optic fields with specific intensity or polarization patterns were obtained. As a consequence, optically tunable FDs emerged, whose morphologies as well as their $U_{\rm c}$ could be freely controlled.

Our work shows how the combination of light tunability of the cholesteric pitch, the voltage tunability of the FDs, and the patterned photo-alignment allow the creation of variable microstructures inside CLCs. With the advantages of remote, instant, precise, and flexible operation by an optical field, a feasible way to tune the microstructures for novel photonic devices has been obtained. For example, we demonstrate prototypes of ring-shaped and fan-shaped gratings that could be switched *in situ*. Their morphologies are tailored by optical-chirality and optical-alignment processes. Such multifunctional gratings may exhibit potential applications in the field of accurate angle measurement.

Note that the system discussed in the paper is not an exclusive solution for the dynamic tuning of cholesteric gratings; several other examples have also been proposed in the literature. They may differ in the host nematic, in the photosensitive chiral dopant (the molecular switch) as well as in the sample geometry and the type of grating. These may include the helical cholesteric structure itself, where the helical axis of a short pitch CLC is parallel to the substrates (uniformly lying helix, ULH);²⁷ the electric field-induced transitions between helical and heliconical structures;²⁸ and electroconvection patterns, whose wave vector is adjustable by simultaneous change of the frequency and amplitude of the applied voltage.²⁶ In each case, the optical tunability is due to the photosensitive dopant, which modifies the helical pitch upon illumination.

II. MATERIALS AND METHODS

A. Samples

Two LC materials were examined and compared. One was an achiral nematic, known as 1008 (4-n-octyloxyphenyl 4-n-methyloxybenzoate). 29,30 Not only its nematic phase exists between the melting point at 63.5 °C and the clearing point at 76.7 °C, but it can be supercooled till 53 °C. It has a negative dielectric anisotropy; the temperature dependence of some material parameters is given in the supplementary material. The other compound was a CLC, obtained by doping the host 1008 with a photosensitive chiral dopant, M5(L) [9-(2-methyl-2,3-dihydro-1H-cyclopenta[a]naphthalen-1-ylidene)-9H-fluorene], 24,25 at a weight concentration of $C_{M5} = 0.025\%$. M5(L) induces a left-handed cholesteric helix. Due to photoisomerization, its helical twisting power $(HTP \approx -4 \times 10^7 \,\mathrm{m}^{-1})$ in the initial dark state²⁵) decreases with the increase in the intensity of blue light ($\lambda = 430 \text{ nm}$) irradiation, resulting in a tunable helical pitch $P(I_{430 \text{ nm}})$. If $I_{430 \text{ nm}}$ rises to the critical point $I_c = 1.14 \text{ mW cm}^{-2}$, the HTP becomes zero, i.e., the helical structure fully unwinds yielding a nematic-like, compensated cholesteric state with $|P(I_c)| = \infty$. It was found, however, that increasing $I_{430~\mathrm{nm}}$ above I_{c} has not resulted in a further change in the HTP, i.e., the system saturated at HTP = 0, corresponding to the nematic-like state. This phenomenon is very different from what we had observed under UV light ($\lambda = 365 \text{ nm}$) irradiation.²⁵ In the latter case, when the UV light intensity exceeded the critical point, M5 underwent a chiral inversion, switching from the left-handed sense to the right-handed one. In any case, HTP returns in a few seconds to its initial value after stopping the illumination.

Two kinds of cells, each with a thickness $d=6\,\mu\mathrm{m}$, were prepared. Both were of a hybrid-aligned (HA) configuration but differed in their planar surface alignment: while one substrate was treated with PI Nissan 7511L to achieve homeotropic alignment, ²⁶ the other, planar substrate was covered either with the non-photosensitive polyimide (PI) Nissan SE150 and rubbed to obtain a uniform in-plane alignment $\mathbf{n_0}$ (standard HA cell), or with the photosensitive layer ^{31,32} and treated via photo-alignment technique to acquire customized in-plane aligning patterns (patterned HA cell).

Samples made of standard and patterned HA cells filled with the nematic 1008 were used to demonstrate the surface effect of the optical field, whereas the sample made of a standard HA cell filled with the photosensitive, chiral, doped 1008 served to demonstrate the bulk effect of the optical field. The dopant concentration used here results in a helical pitch $P\gg d$, yielding a slightly twisted director structure with the twist angle lower than $\pi/2$, ensuring the observability of FDs. Note that for shorter ($P\leq d$) pitches, no FDs are present; instead, a flexoelectrooptic effect $^{33-35}$ develops by the applied voltage.

In order to generate FDs, an electric field perpendicular to the substrates was applied by an amplified dc voltage of a signal generator. Meanwhile, the temperature of the samples was kept constant at $T=60\,^{\circ}\mathrm{C}$ by using a Linkam LTS 450 heating stage, which was controlled by a TMS 94 temperature controller.

The formation and transformation of FDs were monitored by a polarizing microscope (POM) or by an optical setup equipped with a (digital micro-mirror device) DMD, where the samples were placed between crossed polarizers and observed in transmission mode using white light illumination.

18 June 2025 07:10:28

B. Optical setup 1: LCoS technique (λ = 405 nm) for photo-alignment to induce surface effect

The patterned HA cells, with specific surface alignment distribution and anchoring energy, were fabricated by the photoalignment technique, as shown in Fig. 1(a). A polarization-sensitive sulfonic azo-dye, SD1,31 was used as the photo-aligning agent on the planar substrate. This layer (with an approximate thickness of 10 nm) was illuminated by a blue light ($\lambda = 405$ nm) reflected from an liquid crystal on silicon (LCoS) spatial light modulator (SLM). Due to photoisomerization and dichroic absorption, SD1 molecules tend to orient perpendicularly to the local polarization of the illuminating blue light ($\lambda = 405 \text{ nm}$). Subsequently, they guide the CLC director at the surface to realign along the direction of SD1, i.e., perpendicular to the polarization direction of light, through intermolecular interactions. In the setup, the LCoS serves as a uniaxial phase retarder, whose phase retardation δ depends on the applied voltage. Consequently, the output light is linearly polarized, with its polarization direction oriented at an angle of $\delta/2$. Since the phase retardation can be precisely controlled at the pixel level in the LCoS, an arbitrary two-dimensional (2D) polarization direction distribution can be generated on the sample. 36,37 In our experiment, a photomask with pre-designed gray-level pictures was uploaded to the LCoS, resulting in a radial polarization distribution map. Thus, the surface directors of the CLC form the designed tangential in-plane (azimuthally distributed) configuration.

The anchoring energy, provided by the SD1 layer, depends strongly on the exposure dose. Usually, the higher the dose, the stronger the anchoring energy. ^{38,39} Theoretical considerations imply that the anchoring energy is proportional to the order parameter *S* of the SD1 layer, while a longer exposure time and/or a higher dose enhance *S*, resulting in a better alignment uniformity and stronger anchoring ability of SD1. ^{40,41} The increase in the order parameter *S* with the exposure time has been experimentally proven by the observation that the photo-induced phase retardation of the SD1 layer increases with the exposure time.

In our experiment, the intensity $I_{405 \text{ nm}}$ of 14 mW/cm^2 was fixed, while the exposure time t_{ex} was adjusted to 10, 30, and

60 min to change the dose and, thus, to examine the effect of the alignment strength on the formation of FDs.

Regarding sample fabrication, first, the ITO glass substrates underwent ultrasonic and UV-ozone cleaning. Subsequently, they were spin-coated with the photoaligning agent SD1 (0.3 wt. % dissolved in N,N-dimethylformamide). After that, the SD1 layer was cured at 100 °C for 10 min to remove the solvent. Finally, the two substrates (one for homeotropic and the other for photoaligned planar alignment) were assembled together and sealed with epoxy glue, while the cell gap was maintained by spacers of $6.0\,\mu\mathrm{m}$.

C. Optical setup 2: DMD technique (λ = 430 nm) for photo-tuning to induce bulk effect

In addition, in order to imprint the desired space-variant helical structure of CLCs, a dynamic mask photo-tuning technique based on DMD was employed. In this technique, the pre-set intensity-patterned images were uploaded as gray photomasks into the DMD [Fig. 1(b)].⁴²

A collimated blue beam with wavelength $\lambda = 430$ nm, acting as the commanding light, was reflected onto the DMD and subsequently illuminated the sample according to the designed light intensity pattern. Meanwhile, the morphologies of the samples were monitored by a CCD camera, where collimated white light and polarizers were used. 43

It should be noted that, due to the absorption spectra of SD1, the illumination by $\lambda = 430$ nm light cannot modulate the aforementioned surface photo-alignment already produced by $\lambda = 405$ nm light. Instead, the introduction of the $\lambda = 430$ nm light could only affect the *HTP* of the chiral M5(L) within the LC film.

III. EXPERIMENTAL RESULTS

A. Optically induced surface effect tested by the photo-alignment technique

In the following, the photo-tunability of FDs was investigated by changing the surface conditions, either the surface alignment pattern or the anchoring energy.

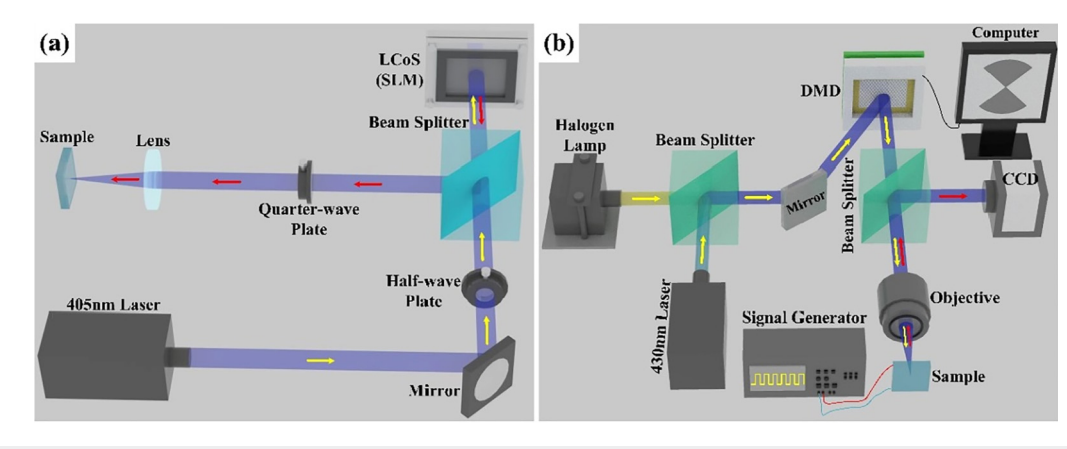


FIG. 1. Schematic diagrams of (a) the LCoS and (b) the DMD setups, which were used to perform the photo-alignment and the photo-tuning, respectively.

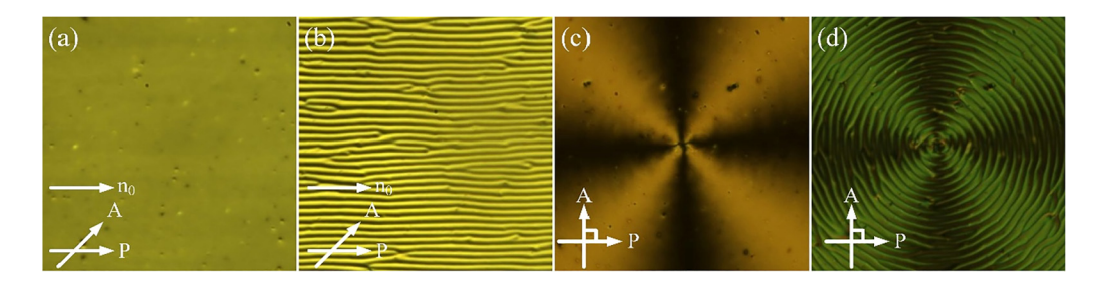


FIG. 2. Snapshots $(300 \times 300 \,\mu\text{m}^2)$ of the unperturbed states at (a) rubbed and (c) photo-aligned planar surfaces, respectively; the corresponding FD states with (b) $U_c = 34.5 \text{ V}$, $\Lambda = 9.1 \,\mu\text{m}$ and (d) with $U_c = 34.0 \,\text{V}$, $\Lambda = 9.3 \,\mu\text{m}$.

1. Dependence of the FD morphology on the photoalignment pattern with strong anchoring

In the absence of an electric or optical field, the well-defined textures of the unperturbed state of the nematic 1008 could be clearly observed in POM. Figure 2(a) shows the homogeneous state in a standard, rubbed HA cell, while Fig. 2(c) exhibits the circular, tangential director orientation of a patterned HA cell, created by photo-alignment using the LCoS setup producing an illumination with a cylindrically symmetric, radial polarization pattern.

When the samples were driven by a dc field only, FD developed if the applied voltage $U_{\rm dc}$ exceeded $U_{\rm c}$. In the two cells, FDs manifested themselves as different morphologies, in agreement with the different alignment configurations at the planar side: in Fig. 2(b), a regular array of parallel stripes along $\mathbf{n_0}$ were observed, while in Fig. 2(d), a regular array of circular stripes were observed.

Both kinds of morphologies appeared, however, around the same U_c in Figs. 2(b) and 2(d), indicating that U_c is independent of the surface alignment pattern.

2. Dependence of $U_{\rm c}$ on the anchoring strength via optical exposure time

The surface anchoring energy of photo-alignment on the azo layer strongly depends on the irradiation dose. That is, at constant intensity, the exposure time $t_{\rm ex}$ determines the anchoring

energy. Usually, the higher the dose, the stronger the anchoring energy. To explore the relation between anchoring strength and FD characteristics, $I_{405~\rm nm}=14~\rm mW/cm^2$ was kept constant, while three typical exposure times $t_{\rm ex}$ were selected. The illumination occurred in a circular spot, whose diameter was gradually reduced. By that, an array of an outer ring (1), a middle ring (2), and a central circle (3) was created, with corresponding exposure times of $t_{\rm ex}=10$, 30, and 60 min, respectively (Fig. 3).

It was observed that while the morphology of FD was independent of the anchoring energy, the $U_{\rm c}$ of FDs was affected by it, as shown in Fig. 3. It is evident that the longer the exposure time, the stronger the resultant anchoring energy, and the higher $U_{\rm c}$. Thus, ring 1, ring 2, and central circle 3 correspond to weak, medium, and strong anchoring, respectively.

3. The dependence of FD morphology on the electric field with strong anchoring

With the above-mentioned surface alignment patterns, the effect of $U_{\rm dc}$ on the FD morphology could be examined. As the voltage increases (decreases), the corresponding circular stripe morphology undergoes shrinkage (expansion), as shown in Figs. 4(a) and 4(b). In other words, an increase in $U_{\rm dc}$ leads to a decrease in the periodicity Λ (the difference in the radius of neighboring circular stripes), and vice versa. Λ was determined by measuring the

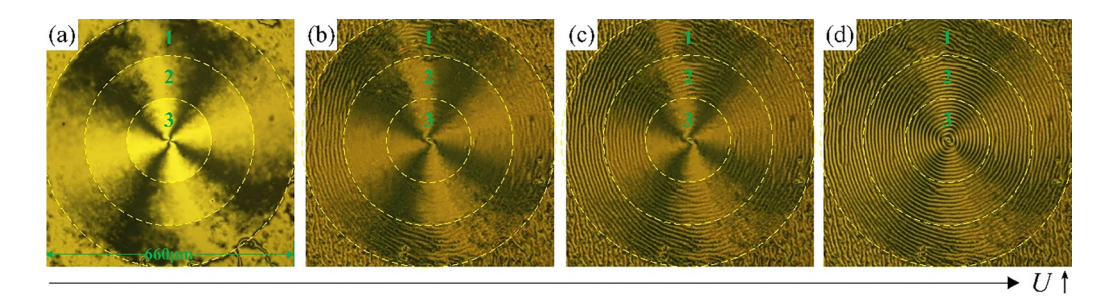


FIG. 3. Snapshots $(600 \times 600 \, \mu\text{m}^2)$ demonstrating the dependence of U_c of FDs on the exposure time t_{ex} , where ring 1, ring 2, and circle 3, separated by dashed circular lines, represent different regions with t_{ex} = 10, 30, and 60 min, respectively. Here, the snapshots represent (a) the unperturbed state; and the patterns slightly above the onset of FDs in the different regions: (b) U_c = 32.9 V in ring 1, (c) U_c = 33.4 V in ring 2, and (d) U_c = 34 V in circle 3. The corresponding periodicity Λ is almost the same, ranging between 9.0 and 9.3 μ m.

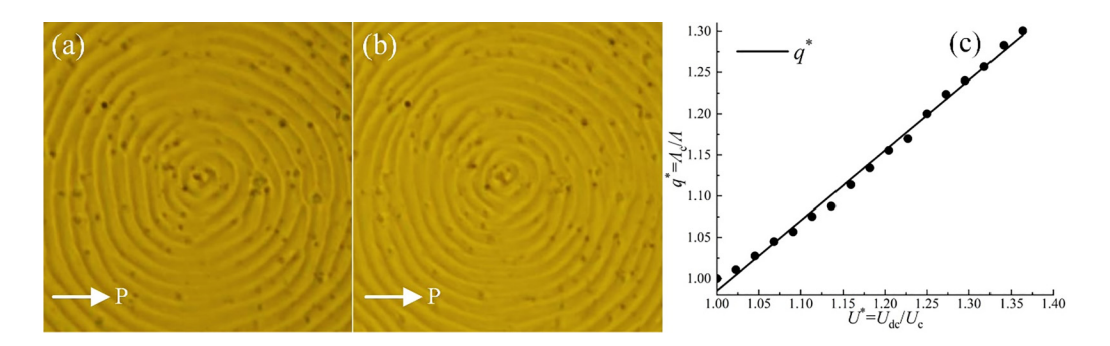


FIG. 4. Representative snapshots of circular FDs at (a) $q^* = 1.05$ and $U^* = 1.1$ and (b) $q^* = 1.24$ and $U^* = 1.3$, with only one polarizer **P** used. (c) Linear dependence of the reduced wavenumber $q^{*} = \Lambda_c/\Lambda$ on the reduced voltage $U^* = U_d/U_c$. Discrete points are measured data, while the straight line was obtained by fitting.

width of at least 10 stripes and dividing by the actual number of stripes. Then, the reduced wavenumber $q^* = \Lambda_c / \Lambda$ was calculated and plotted in Fig. 4(c) as a function of reduced voltage $U^* = U_{dc}/U_c$. Here, $U_c = 34.0 \text{ V}$ corresponds to the threshold voltage of FDs, while $\Lambda_c = 9.3 \,\mu\text{m}$ is the critical periodicity at FD onset. Note that the linear increase in the wavenumber with the voltage is a typical behavior of flexoelectric domains. 15 It is due to the fact that shrinking Λ results in higher flexoelectric polarization; thus, the flexoelectric interaction can compensate larger deformation free energies.

4. Application of the circular FDs: Circular ring diffraction grating

The periodic director distortion of FDs corresponds to an optical grating that is capable of diffracting an incident beam. The aforesaid tunability of FDs, enabled by electric field and photoalignment, can be exploited to design new kinds of controllable diffraction gratings.

Herein, a prototype grating composed of concentric circular stripes demonstrates variable far-field diffraction fringes depending on the applied U_{dc} , as shown in Fig. 5, using a He-Ne laser ($\lambda = 633 \text{ nm}$) diffraction technique. The radius R_1 of the first-order fringe detected at a diffraction distance of L = 10 cm defines the firstorder diffraction angle θ_1 via $\tan \theta_1 = R_1/L$.

It should be noted that, unlike traditional linear gratings, our grating had circular spatial symmetry. Hence, a circularly polarized laser was used to explore the diffraction effect of this new circular stripe grating. It was observed that under these conditions, the diffractive fringes are also circles.

Figures 5(a) and 5(b) illustrate that the fringes depend on the applied voltage. Figure 5(c) depicts the dependence of the reduced radius $R_1^* = R_1/R_c$ on the reduced voltage $U^* = U_{dc}/U_c$. Here, R_1 and R_c correspond to the radius of the first-order diffractive circular ring at U_{dc} and at U_c , respectively. The radius R_1 is related to $\vec{\sigma}$ the periodicity Λ of FDs via $\Lambda \sin \theta_1 = \lambda$. For small diffraction angles θ_1 , this means a linear relation between R_1 and Λ^{-1} . Thus by applying an appropriate voltage, the periodicity Λ of the grating can be precisely controlled. In addition, such an operation can be completed dynamically.

B. Optically induced bulk effect by the photo-tunable chirality

Photo-tunability of FDs was investigated in standard HA cells with a uniform planar surface alignment achieved through rubbing.

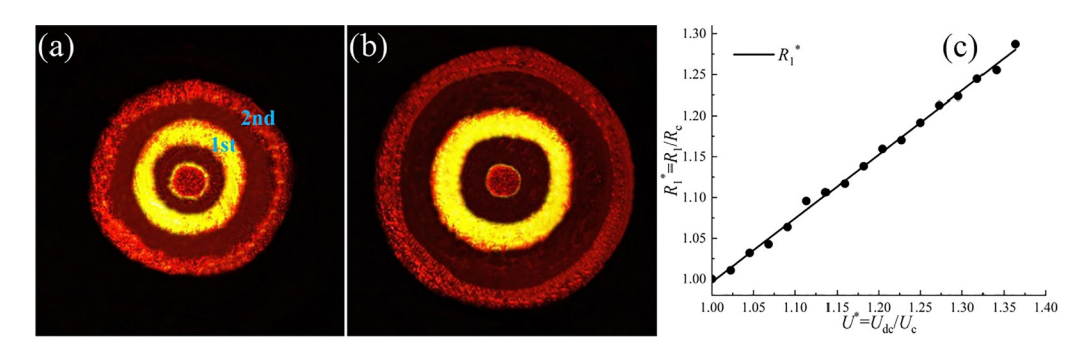


FIG. 5. Typical dc voltage-dependent diffraction fringes: (a) at U* = 1.1, R₁* = 1.06; (b) at U* = 1.3, R₁* = 1.22; (c) the linear dependence of R₁* = R₁/R_c on the reduced voltage $U^{\epsilon} = U_{dd}/U_{c}$. Here, R_1 and R_c represent the radius of the first-order diffractive circular rings at U_{dc} and at U_{c} , respectively, at a diffraction distance of L = 10 cm. Discrete points are measured data, while the straight line was obtained by fitting.

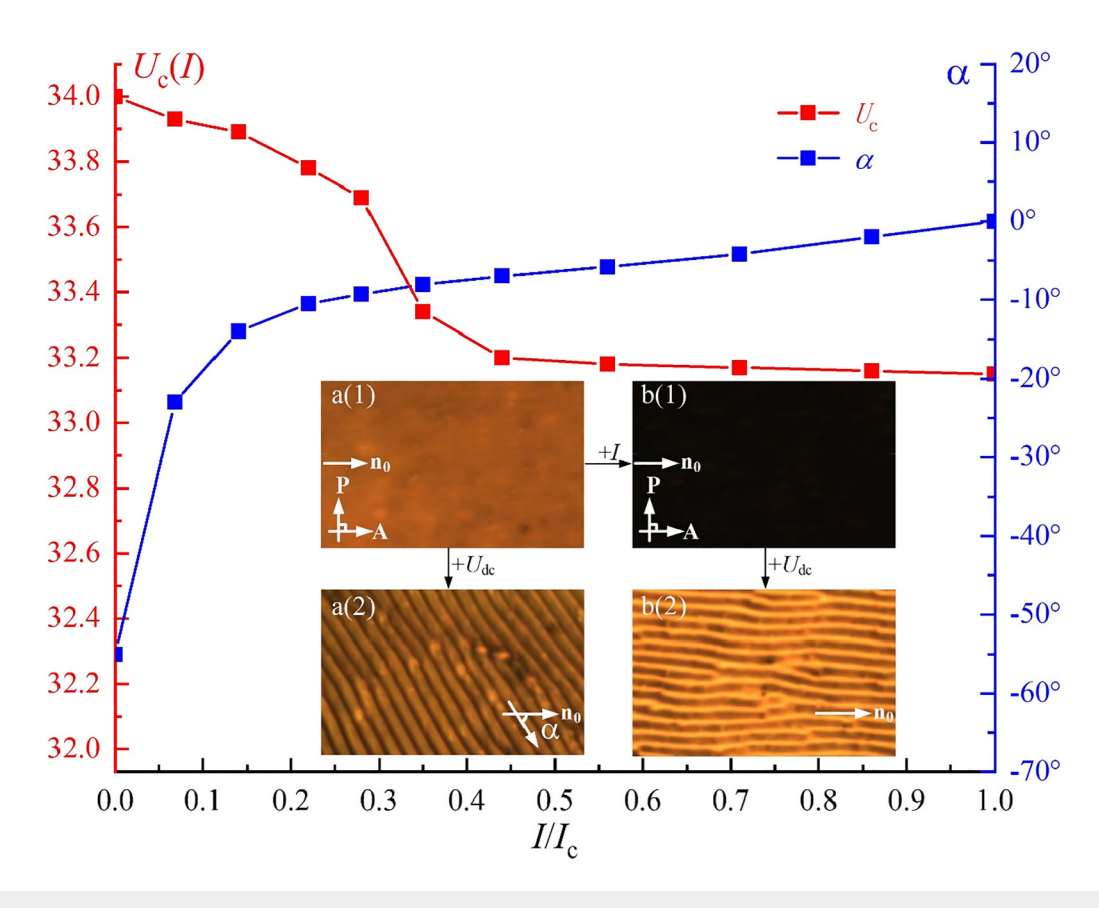


FIG. 6. Dependence of the light-driven rotation angle α and the threshold voltage U_c on the light intensity $I_{430~nm}$, each after 60 s of illumination. Here, the inset snapshots (145 × 230 μm) a(1) and b(1) are representative textures of the pattern-free states with crossed polarizer **P** and analyzer **A**, illuminated in the absence of the electric field by $I_{430~nm}$ = 0 and $I_{430~nm}$ = I_c , respectively; inset snapshots a(2) and b(2) are the FD patterns slightly above the onset, at $U_{dc} = U_c = 34.0 \text{ V}$, $I_{430~nm} = 0$ (in the absence of illumination) and $U_{dc} = U_c = 33.2 \text{ V}$, $I_{430~nm} = I_c = 1.14 \text{ mW/cm}^2$ (after being illuminated), respectively.

The cell was filled with the photosensitive CLC material, which allowed the utilization of the photoinduced chirality in the bulk LC film. Upon uniform illumination with a blue (λ = 430 nm) light, the dc voltage-induced FDs change in response. It was observed that both $U_{\rm c}$ and the orientation of the FD stripes vary according to the intensity $I_{\rm 430~nm}$, as illustrated in Fig. 6.

1. Effect of the intensity $I_{430 \text{ nm}}$ on the orientation of FDs

In Sec. III A 3, we demonstrated that the periodicity Λ of FDs could be strongly modulated by dc field. Herein, we demonstrate that when the combined effect of $\lambda = 430$ nm optical and dc electrical fields is present, the morphology of FDs undergoes a transformation, manifested in rotated stripes.

It was observed that during the whole light irradiation period, FDs always appeared as straight stripes; however, the direction of the stripes (represented by the angle α between the stripes and the rubbing direction $\mathbf{n_0}$) alters with different intensity $I_{430~\mathrm{nm}}$. Initially, when $I_{430~\mathrm{nm}} = 0$, $\alpha = -\alpha_0$. Afterward, as $I_{430~\mathrm{nm}}$ grows to I_{c} the stripes rotate counterclockwise and the corresponding α gradually

increases from $-\alpha_0$ until $\alpha=0$, making α dependent on $I_{430~\mathrm{nm}}$. At this point, the direction of the stripes is parallel to $\mathbf{n_0}$. It is thought that the alteration of the helical pitch due to light irradiation is responsible for such an effect.

For comparison, in order to prove the effect of alteration of the helical pitch, we separately inspected the evolution of the sample morphology under $\lambda=430\,\mathrm{nm}$ light in the absence of the electric field. When $I_{430\,\mathrm{nm}}$ is in the range of $0 \le I_{430\,\mathrm{nm}} < I_{\odot}$ the system is in left-handed helical states with $P(I_{430\,\mathrm{nm}}) < 0$, yielding uniform textures with different colors [see an example in inset a(1) in Fig. 6]. If $I_{430\,\mathrm{nm}} = I_{\odot}$, one finds a complete light extinction at crossed polarizers, corresponding to the unwound, compensated CLC state with $P(I_{\rm c}) \approx \infty$, shown in inset b(1) in Fig. 6.

2. Dependence of U_c on $I_{430\;nm}$ via the alteration of the helical pitch

The $U_{\rm c}$ of FDs is also influenced by the light intensity $I_{430~\rm nm}$. The higher the $I_{430~\rm nm}$, the lower the $U_{\rm c}(I_{430~\rm nm})$. Eventually, $U_{\rm c}(I_{430~\rm nm})$ decreased to the value as that in the pure nematic case when $I_{430~\rm nm}=I_{\rm c}$.

By examining the curves how α and $U_{\rm c}$ vary with $I_{430~\rm nm}$ (Fig. 6), it can be inferred that these two characteristics are connected. Since both of them are functions of the pitch P, the adjustment of P by $I_{430~\rm nm}$ makes them light intensity-dependent.

In addition to α and U_c , the diffraction efficiency η , defined as the ratio of the intensity of the ±1st-order diffracted beam to the intensity of the incident beam is also an important parameter of FD gratings. In principle, η may also depend on the illuminating intensity $I_{430~\rm nm}$, as α and U_c do. Using a 633 nm circularly polarized laser, it was observed that the diffraction spots also relocate corresponding to the rotation of the grating; however, the diffraction efficiency η remains almost unchanged. As a representative example, for the gratings in Figs. 6(a2) and 6(b2), $\eta \approx 12.5\%$.

3. Demonstration of optical-addressing

As an intuitive application to demonstrate the optically induced bulk effect, we used the optical-addressing technique to display a customized image, as shown in Fig. 7. Again, this is the consequence of the reduction of $U_{\rm c}$ in the illuminated area, while $U_{\rm c}$ remained unchanged in the unilluminated regions. In this way, the distribution of FD stripes is consistent with the spatial profile of the light intensity.

In addition, due to the tunability of the pitch, the carried information could be erased and rewritten into FD stripes on-demand by optical-addressing.

IV. DISCUSSION

So far the theoretical description of the flexoelectric effect mainly constrained on the behavior in planar samples. The threshold voltage U_c and the critical wavenumber $q_c = 2\pi/\Lambda_c$ were derived in linear approximations, $^{8-11,13}$ while the voltage dependence of the wavenumber q(U) was calculated by nonlinear theories. 15,16,44 Unfortunately, similar theoretical treatments for the geometries used here—hybrid-aligned nematics with finite anchoring energy or hybrid-aligned cholesterics—are not yet available. Although the generalization of the theoretical description might be straightforward, the calculations are tedious and demanding; thus, it cannot be part of the present paper. Therefore, we can only compare our observations with those obtained for other geometries.

A. Optically induced surface effect

Our experimental results indicate that both the morphology and the critical voltage of FDs can be influenced by the surface conditions. For the nematic 1008 in a *photo-aligned* patterned HA cell, the FDs grow along the local director orientation at the planar surface, forming circular stripes according to the circular tangential surface alignment pattern. It should be stressed that, even in the presence of a surface alignment pattern, the nematic film does not form a helical structure spontaneously, because one substrate possesses an azimuthally degenerate vertical alignment. Thus, the whole system always maintains the nematic state, where each part in the space orients along the local planar alignment on the surface. If the alignment distribution degrades to a uniform orientation, as in the rubbing case, then the FD stripes turn into parallel ones along \mathbf{n}_0 . Such changes have a negligible effect on the magnitude of the elastic energy, and on the coupling energy between the polarization $\mathbf{P}_{\rm fl}$ and the electric field, thus, the critical voltage $U_{\rm c}$ does not change as seen in Fig. 2.

The influence of surface anchoring energy on FDs in HA nematics is surely a new observation. Previous theoretical attempts to describe the $U_{\rm c}$ of FDs in HA cells assumed strong surface anchoring. ^{45,46} Finite anchoring energy was theoretically considered only for planar samples ^{47,48} predicting a decrease of $U_{\rm c}$ and some modification of $q_{\rm c}$ at reducing anchoring strength. These predictions are in line with our experimental results, which evidently proved that $U_{\rm c}$ is higher in regions with higher anchoring strength (see Fig. 3). Furthermore, the linear increase of q* with the voltage (Fig. 4) matches the theoretical predictions obtained for planar samples. ^{15,16,44}

B. Optically induced bulk effect

The optically induced bulk effect was studied in the rubbing-aligned standard HA cell, filled with a long pitch CLC (1008 doped with M5). Theoretical description of FDs in CLCs is still an unexplored field. One of its reasons might be that FDs are expected to occur only in long pitch CLCs (in slightly chiral nematics). Instead, studies mostly focused rather on short pitch CLCs, where another, homogeneous deformation—the flexoelectrooptic effect^{33–35} occurs due to flexoelectricity.

FDs were tested in a twisted planar nematic configuration. The calculations yielded higher U_c than in the untwisted planar case and a slight, polarity dependent deviation of the direction of the FD stripes from the initial director at the midplane of the cell. FDs were also studied in a planar nematic under the magnetic field-induced twist Freedericksz transition. The twist deformation due to the magnetic field resulted in U_c and Q_c increasing with the magnetic field above the Freedericksz threshold (i.e., with

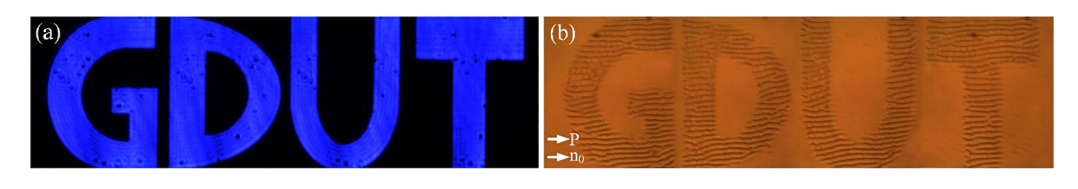


FIG. 7. (a) The photomask and (b) the resulting customized information composed of FD stripes at uniform rubbing alignment, with a size of 490 × 145 μ m². Here, U_{dc} = 33.3 V and $I_{430 \text{ nm}} = I_c$. "GDUT" is the abbreviation of the affiliation of the submitting author.

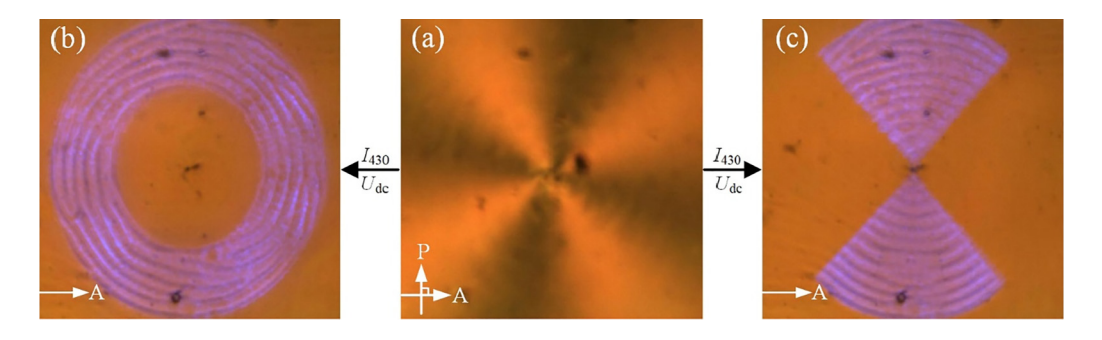


FIG. 8. (a) The initial unperturbed texture and (b) the hollow ring-shaped grating and (c) the fan-shaped grating produced from the unperturbed state by the combined action dc electric and λ = 430 nm light fields at $U_{\rm dc}$ = 33.5 V and $I_{\rm 430}$ = $I_{\rm c}$ = 1.14 mW/cm². In the figure, there is a superimposed faint blue background demonstrating the intensity pattern of the λ = 430 nm commanding beam. The snapshot size is 150 × 150 μ m².

increasing twist deformation) while the FD stripe direction roughly followed the maximum twist angle.

Our experimental results showed that FDs in CLCs are always present in the form of parallel stripes whose orientation, however, deviates from the rubbing direction \mathbf{n}_0 . In addition, the characteristics of FDs in CLC can be adjusted upon the application of an optical field.

In a hybrid cell, the LC director is fixed on the planar substrate, while the vertical alignment on the other substrate is azimuthally degenerate, i.e., it does not restrict any twist along the vertical axis. Since the director can rotate freely at the vertical alignment surface, the values of the pitch P of the CLC system are equal throughout the whole cell space. This holds true for both the dark state $P(I_{430 \text{ nm}} = 0) = P_0$ (P_0 is the natural pitch) and the illuminated states, where $P(I_{430 \text{ nm}} > 0) \ge P_0$.

If an appropriate U_{dc} is applied, FDs appear with periodic stripes, whose orientation depends on the twisted director structure. Based on the observations and simulations for the twisted planar structures, ^{49,30} it is expected that the stripes should be parallel to the orientation corresponding roughly to the director in the midplane of the cell, at an azimuthal angle of about half of the total director twist. As the helical pitch P varies with $I_{430 \text{ nm}}$, accordingly the azimuthal angle in the midplane changes as well, resulting in rotated FD stripes.

These conclusions are in full agreement with our experimental findings shown in Fig. 6, implying that the change in the stripe direction angle α and the change in the critical U_c are the consequence of the alteration of the helical pitch P. With enhanced $I_{\rm 430~nm}$, HTP decreases, P increases, $U_{\rm c}$ and the deviation of the stripe direction from $\mathbf{n_0}$ reduce. Eventually, at $P \to \infty$, the CLC system approaches the nematic system, and the corresponding characteristics of FDs evolve into the familiar forms of the nematic system.

Hence, the modulation of P by $\lambda = 430$ nm light is the precondition for the tunability. In order to clarify the role of chirality in the formation of oblique FDs, by varying the intensity and profile of the stimulating light, quantitative functional relationships [such as $\alpha(P)$ and $U_c(P)$] can be acquired, providing a new method to verify the theoretical model based on free energy.

V. APPLICATION SCENARIOS: THE SYNERGISTIC EFFECT OF THE OPTICALLY INDUCED SURFACE EFFECT AND THE OPTICALLY INDUCED BULK EFFECT

Utilizing photo-aligned cells and a photo-chirality-switching CLC material, by appropriately selecting the surface alignment patterns and the irradiation light intensity patterns, prototype photonic devices based on arbitrary, topologically circular-stripeshaped FD structures can be fabricated. These devices lead to unconventional diffraction gratings with specific functions. Herein, two kinds of prototypical gratings, the hollow ring-shaped grating Such gratings can be embedded into emerging angle encoders to accurately measure angles, for instance, for adjusting the altitude of accurately measure angles, for instance, for adjusting the altitude of drones and measuring the angles of the rotating shafts of computer numerical control (CNC) machines.

VI. CONCLUSION

We investigated the appearance of FDs in a CLC under an electric field and showed that the corresponding morphology and critical voltage can be modulated by the optically induced surface and bulk effects, with the help of photo-alignment and phototuning techniques, respectively. We further demonstrated the dualmode operations (either electric field only or combined electric and optical fields) of prototype devices based on such tunability. With customized patterns and desired switching, adjustable FDs may open new perspectives and provide yet unseen photonic functionalities. For example, they may become promising candidates to replace the fixed ring gratings in altitude monitoring for autopilot systems.

SUPPLEMENTARY MATERIAL

See the supplementary material for the parameters of 1008.

ACKNOWLEDGMENTS

This work was supported by the Joint Fund for Regional Innovation and Development of National Natural Science Foundation of China (NNSFC) (No. U24A2078) and by the Hungarian National Research, Development, and Innovation Office under Grant Nos. NKFIH FK142643 and 2023-1.2.1-ERA NET-2023-00008. P.S. acknowledges the support by the János Bolyai Research Scholarship of the Hungarian Academy of Sciences (HAS). A.B. acknowledges the hospitality of the Guangdong University of Technology.

AUTHOR DECLARATIONS

Conflict of Interest

The authors have no conflicts to disclose.

Author Contributions

Weipeng Peng: Funding acquisition (equal). Fei Liang: Resources (equal). Yangquan Liao: Methodology (equal). Hongzhen Jing: Methodology (equal). **Ying Xiang:** Supervision (equal); Visualization (equal). **Péter Salamon:** Investigation (equal); Methodology (equal). Nándor Éber: Data curation (equal). Ágnes Buka: Investigation (equal). Ling Wang: Methodology (equal). Nemanja Trišović: Methodology (equal). Huaiping Zhang: Supervision (equal).

DATA AVAILABILITY

The data that support the findings of this study are available from the corresponding authors upon reasonable request.

REFERENCES

- ¹D. K. Yang and S. T. Wu, Fundamentals of Liquid Crystal Devices (John Wiley & Sons, Ltd., 2014).
- ²L. M. Blinov and V. G. Chigrinov, Electrooptic Effects in Liquid Crystal Materials (Springer, New York, 1994).
- ³N. Éber, P. Salamon, and Á Buka, "Electrically induced patterns in nematics and how to avoid them," Liq. Cryst. Rev. 4, 101-134 (2016).
- ⁴Z. Y. Zhou, X. F. Zhang, S. Halder, L. Hu, and D. K. Yang, "Bistable polymerstabilized cholesteric-liquid-crystal window based on flexoelectric and dielectric effects," Phys. Rev. Appl. 21, 024045 (2024).
- ⁵Y. Li and S. T. Wu, "Advancing from scalar to vectorial liquid crystal holography: A paradigm shift," Light Sci. Appl. 13, 207 (2024).
- ⁶M. Y. Xu, H. Z. Jing, Y. Xiang, Y. K. Liu, Z. G. Cai, F. J. Wang, J. Y. Li, E. Wang, Y. Q. Wang, and Y. H. Cai, "Voltage selectable dual-mode optically-induced grating in ZnTPP doped chiral nematic liquid crystals," Opt. Mater. Express 7, 1317 (2017).
- ⁷A. Ryabchun and A. Bobrovsky, "Cholesteric liquid crystal materials for tunable diffractive optics," Adv. Opt. Mater. 6, 1800335 (2018).
- ⁸B. R. Meyer, "Piezoelectric effects in liquid crystals," Phys. Rev. Lett. 22, 918-921 (1969).
- ⁹Á Buka, T. Tóth-Katona, N. Éber, A. Krekhov, and W. Pesch, "Chapter 4. The role of flexoelectricity in pattern formation," in Flexoelectricity in Liquid Crystals. Theory, Experiments and Applications, edited by Á Buka and N. Éber (Imperial College Press, London, 2012), pp. 101-135.
- 10S. A. Pikin, Structural Transformations in Liquid Crystals (Gordon and Breach Science Publishers, New York, 1991).
- $^{\mathbf{11}}\mathrm{Y}.$ P. Bobylev and S. A. Pikin, "Threshold piezoelectric instability in a liquid crystal," Sov. Phys. JETP 45, 195 (1977).
- 12M. I. Barnik, L. M. Blinov, A. N. Trufanov, and B. A. Umanski, "Flexo-electric domains in liquid crystals," J. Phys. (France) 39, 417 (1978).
- $^{\boldsymbol{13}}\text{A}.$ Krekhov, W. Pesch, and Á Buka, "Flexoelectricity and pattern formation in nematic liquid crystals," Phys. Rev. E 83, 051706 (2011).

- ¹⁴P. Salamon, N. Éber, A. Krekhov, and Á Buka, "Flashing flexodomains and electroconvection rolls in a nematic liquid crystal," Phys. Rev. E 87, 032505 (2013).
- 15W. Pesch, A. Krekhov, N. Éber, and Á Buka, "Nonlinear analysis of flexodomains in nematic liquid crystals," Phys. Rev. E 98, 032702 (2018).
- ¹⁶Q. H. Han, S. J. Elston, W. Kamal, L. P. Xue, and S. M. Morris, "A nonlinear model of flexoelectric liquid crystal diffraction gratings," Opt. Laser Technol. 180, 111502 (2025).
- 17Y. H. Shin, Z. Y. Zhou, S. Halder, X. F. Zhang, and D. K. Yang, "Reconfigurable liquid crystal diffraction grating based on flexoelectric effect," J. Mol. Liq. 357, 119150 (2022).
- 18Y. Xiang, H. Z. Jing, Z. D. Zhang, W. J. Ye, M. Y. Xu, E. Wang, P. Salamon, N. Éber, and Á Buka, "Tunable optical grating based on the flexoelectric effect in a bent-core nematic liquid crystal," Phys. Rev. Appl. 7, 064032 (2017).
- 19 M. Y. Xu, M. J. Zhou, Y. Xiang, P. Salamon, N. Éber, and Á Buka, "Control of light polarization by optically-induced-chirality in photosensitive nematic fluids," Opt. Express 23, 15224 (2015).
- 20 H. Z. Jing, M. Y. Xu, Y. Xiang, E. Wang, D. F. Liu, A. Poryvai, M. Kohout, N. Éber, and Á Buka, "Light tunable gratings based on flexoelectric effect in photoresponsive bent-core nematics," Adv. Opt. Mater. 7, 1801790 (2019).
- ²¹V. G. Chigrinov, V. M. Kozenkov, and H. S. Kwok, *Photoalignment of Liquid* Crystalline Materials: Physics and Applications (John Wiley & Sons, 2008).
- ²²W. Ji, B. Y. Wei, P. Chen, W. Hu, and Y. Q. Lu, "Optical field control via liquid crystal photoalignment," Mol. Cryst. Liq. Cryst. 644, 3-11 (2017).
- ²³Y. Xiang, H. Z. Jing, W. Y. Sun, H. Chen, G. Cipparrone, P. Pagliusi, M. Xua, and G. H. Huang, "Topological defects arrays and control of electro-convections in periodically photo-aligned bent-core nematics," J. Mol. Liq. 318, 114058 (2020). ²⁴J. Sun, L. Yu, L. Wang, C. Li, Z. Yang, W. He, C. Zhang, L. Zhang, J. Xiao, X. Yuan, F. Lie, and H. Yang, "Optical intensity-driven reversible photonic bandgaps in self-organized helical superstructures with handedness inversion," J. Mater. Chem. C 5, 3678 (2017).
- 25H. Z. Jing, Y. Xiang, M. Y. Xu, E. Wang, J. Wang, N. Éber, and Á Buka, "Light-controllable electroconvection patterns in a chiral nematic liquid crystal," Phys. Rev. Appl. 10, 014028 (2018).
- 26Y. Xiang, H. Z. Jing, H. Chen, J. Zhang, X. Y. Ding, J. Y. Li, Z. G. Cai, N. Éber, and Á Buka, "Light-driven rotation of gratings formed by electroconvection patterns in cholesteric liquid crystals," J. Mol. Liq. 337, 116366 (2021).
- ²⁷H. K. Bisoyi, T. J. Bunning, and Q. Li, "Stimuli-driven control of the helical axis of self-organized soft helical superstructures," Adv. Mater. 30, 1706512 (2018).
- ²⁸C.-L. Yuan, W. Huang, Z.-G. Zheng, B. Liu, H. K. Bisoyi, Y. Li, D. Shen, Y. Lu, and Q. Li, "Stimulated transformation of soft helix among helicoidal, heliconical, and their inverse helices," Sci. Adv. 5(10), eaax9501 (2019).
- ²⁹G. G. Nair, C. A. Bailey, S. Taushanoff, K. Fodor-Csorba, A. Vajda, Z. Varga, A. Bóta, and A. Jákli, "Electrically tunable color by using mixtures of bent-core and rod-shaped molecules," Adv. Mater. 20, 3138 (2008).
- 30 P. Salamon, N. Éber, Á Buka, T. Ostapenko, S. Dölle, and R. Stannarius, "Magnetic control of flexoelectric domains in a nematic fluid," Soft Matter 10, 4487-4497 (2014).
- 31 O. Yaroshchuk, J. Ho, V. Chigrinov, and H.-S. Kwok, "Azodyes as photoalignment materials for polymerizable liquid crystals," Jpn. J. Appl. Phys. A 46, 2995-2998 (2007).
- 32X. M. Yu, T. W. Li, J. X. Sang, M. Xiao, J. H. Shang, and J. T. Sun, "Orientation stabilization of light-controlling layers using liquid crystal polymers," Displays 86, 102893 (2025).
- 33 J. S. Patel and R. B. Meyer, "Flexoelectric electro-optics of a cholesteric liquid crystal," Phys. Rev. Lett. 58, 1538-1540 (1987).
- 34P. Rudquist, L. Komitov, and S. T. Lagerwall, "The flexoelectrooptic effect," rroelectrics 213, 53-62 (1998).
- 35P. Rudquist and S. T. Lagerwall, "Chapter 7. Applications of flexoelectricity," in Flexoelectricity in Liquid Crystals. Theory, Experiments and Applications, edited by Á Buka and N. Éber (Imperial College Press, London, 2012), pp. 211-247.
- 36 Y. Li, Y. D. Liu, S. D. Li, P. C. Zhou, T. Zhan, Q. M. Chen, Y. K. Su, and S. T. Wu, "Single-exposure fabrication of tunable Pancharatnam-Berry devices using a dye doped liquid crystal," Opt. Express 27, 9055 (2019).

- 37B. Berteloot, I. Nys, G. Poy, J. Beeckman, and K. Neyts, "Ring-shaped liquid crystal structures through patterned planar photo-alignment," Soft Matter 16,
- 38 A. K. Srivastava, W. L. Zhang, J. L. Schneider, A. L. Rogach, V. G. Chigrinov, and H. S. Kwok, "Photoaligned nanorod enhancement films with polarized emis-
- sion for liquid-crystal-display applications," Adv. Mater. 29, 1701091 (2017). 39S. Petrov, N. H. M. Chau, V. Marinova, C. C. Sun, K. Y. Hsu, and S. H. Lin, "Controllable LC anchoring on poly{1-[4-(3-carboxy-4-hydroxyphenylazo) benzenesulfonamido]-1,2-ethanediyl, sodium salt}command surface," Polymer **272**, 125841 (2023).
- 40 A. D. Kiselev, V. Chigrinov, and D. D. Huang, "Photoinduced ordering and anchoring properties of azo-dye films," Phys. Rev. E 72, 061703 (2005).

 ⁴¹V. Chigrinov, S. Pikin, A. Verevochnikov, V. Kozenkov, M. Khazimullin,
- J. Ho, D. D. Huang, and H.-S. Kwok, "Diffusion model of photoaligning in azo-dye layers," Phys. Rev. E 69, 061713 (2004).
- ⁴²F. Liang, H. Z. Jing, J. M. Fu, Y. Xiang, P. Salamon, N. Eber, A. Buka, M. Kohout, J. Y. Li, and J. W. Chen, "Controlling diffracted beam-polarization by patterned optical-field in a photosensitive chiral nematic," J. Mol. Liq. 420, 126814 (2025). ⁴³H. Wu, W. Hu, H. C. Hu, X. Lin, G. Zhu, J. W. Choi, V. Chigrinov, and Y. Lu,
- "Arbitrary photo-patterning in liquid crystal alignments using DMD-based lithography system," Opt. Express 20(15), 16684-16689 (2012).

- 44E. M. Terent'ev and S. A. Pikin, "Nonlinear effects in a real flexoelectric structure," Sov. Phys. JETP 56, 587-590 (1982); Zh. Eksp. Teor. Fiz. 83, 1038-1044
- 45V. A. Delev, A. P. Krekhov, and L. Kramer, "Crossover between flexoelectric stripe patterns and electroconvection in hybrid aligned nematics," Mol. Cryst. Liq. Cryst. 366, 849-856 (2001).
- ⁴⁶S. P. Palto, N. J. Mottram, and M. A. Osipov, "Flexoelectric instability and spontaneous chiral-symmetry breaking in a nematic liquid crystal with asymmetric boundary conditions," Phys. Rev. E 75(6), 061707 (2007).
- ⁴⁷M. F. Lednei and I. P. Pinkevich, "Threshold spatially periodic structure of the director in a nematic flexoelectric cell with finite anchoring energy," Crystallogr. Rep. 50, 471-477 (2005).
- ⁴⁸M. Ledney and I. Pinkevych, "Influence of anchoring at a nematic cell surface on threshold spatially periodic reorientation of a director," Liq. Cryst. 34, 577-583 (2007).
- 49 B. A. Umanskii, V. G. Chigrinov, L. M. Blinov, and Y. B. Podyachev, "Flexoelectric effect in twisted liquid-crystal structures," Sov. Phys. JETP 54(4), 694-699 (1981).
- 50H. Z. Jing, H. Chen, J. Zhang, X. Y. Ding, J. Y. Li, Z. G. Cai, N. Éber, and Á Buka, "Light-driven rotation of gratings formed by electroconvection patterns in cholesteric liquid crystals," J. Mol. Liq. 337, 116366 (2021).